

Young stellar population of Bright-Rimmed Clouds 5, 7 and 39

ABSTRACT

Bright-rimmed clouds (BRCs) are sites of triggered star formation. We studied three BRCs (BRC 5, BRC 7 and BRC 39) using optical and infrared observations in order to obtain a census of young stellar objects (YSOs) to infer the star formation scenario in the region. **The spatial distributions of YSOs in the studied BRC regions show aligned distributions. We found the most of the class 0/I sources near/inside the bright rims of the clouds and class II sources widely distributed, providing the qualitative evidences for sequential star formation in small scales. The variation of mean age of the YSOs with respect to the location from the bright rim provide the quantitative support for the small scale sequential star formation in the regions. All of the BRCs contain small grouping of young stars at the head, which in the case of BRC 7 is more prominent and in front of the rim. This favours the idea that triggering due to radiation driven implosion from massive stars is giving birth to the second generation star clusters/groups.**

1 INTRODUCTION

The presence of massive stars has dramatic impact on their immediate vicinity. They emit copious amount of ionizing radiation and carve bright HII regions. The propagating ionization/shock fronts subsequently erode the interfaces between the HII regions and the dense molecular clouds. This process can either curb star formation in the immediate vicinity due to the excavation of dust and gas, or induce the next generation star formation in a phenomenon known as ‘sequential star formation’.

Out of a number of processes which induce the star formation at the periphery of HII regions, two processes quite oftenly observed are : ‘collect & collapse’ and ‘radiation driven

implosion (RDI)’. In the ‘collect and collapse’ scenario, material accumulated by the expanding ionization front (IF) of an HII region becomes gravitationally unstable, so it fragments and collapses to form stars (Elmegreen & Lada 1977). The presence of young stellar objects (YSOs) or massive condensations at the periphery of the HII region is considered as the observational indicator of this process (e.g., Deharveng et al. 2005). In the RDI process a pre-existing dense clump is exposed to the ionizing radiation from massive star(s) and the photoionization induced shock may compress the molecular cloud. The head part of the clump collapses due to the high pressure of the ionized gas and self-gravity, which consequently leads to the formation of next generation stars (e.g., Bertoldi 1989, Lefloch & Lazareff 1995). The anisotropic distribution of the YSOs in and small molecular cloud surrounded by curved bright-rim is the observational signatures of the RDI process (Lee et al. 2005).

Bright-rimmed clouds (BRCs) are small molecular clouds located near the edges of evolved HII regions with the rims facing the ionizing stars of the HII regions. Their physical conditions and morphology match well with the theoretical models of RDI (e.g., Bertoldi 1989) and, therefore, BRCs are generally believed to be the sites of induced star formation. Many BRCs show signatures of recent/ongoing star formation such as Herbig-Haro (HH) objects and Infrared Astronomical Satellite (IRAS) point sources of low temperature that meet the criteria of YSOs. Sugitani, Fukui & Ogura (1991) (hereafter SFO91) and Sugitani & Ogura (1994) compiled catalogues of all together 89 BRCs associated with IRAS point sources for the northern and southern hemispheres. Near infrared (NIR) imaging of many BRCs by Sugitani et al. (1995) revealed elongated aggregates of YSOs with bluer (presumably older) stars closer to the ionizing source as compared to the redder (presumably young stars). Thus they proposed that star formation activity propagates along the axis of the BRCs as the ionization/shock front advances further into the molecular cloud. These authors named it as the ‘small scale sequential star formation (S^4F)’ hypothesis.

Ogura et al. (2007, hereafter referred as *Paper I*) undertook BVI_c photometry of four BRC aggregates (BRCs 11NE, 12, 14 and 37) and showed that the stars inside or on the bright rims tend to have younger ages than those outside, as expected from the S^4F hypothesis. Chauhan et al. (2009, hereafter referred as *Paper II*) extended the study to a few more BRCs and confirmed the S^4F hypothesis.

In order to study the star formation processes, to examine the nature and spatial-age gradients of the stellar populations in BRC regions, we studied BRCs 5, 7 and 39 using

Table 1. Log of optical observations

Region	Telescope	Filter; exposure time(sec) \times No. of frames	Date of observations
BRC 5	ST, Nainital	V : 300 \times 4; I _c : 180 \times 4	2006.10.17
BRC 7	ST, Nainital	V : 300 \times 6; I _c : 300 \times 3	2006.10.27
BRC 39	ST, Nainital	V : 300 \times 2; I _c : 200 \times 2	2006.10.17
BRC 39	HCT, Hanle	V : 300 \times 4; I _c : 200 \times 4	2008.10.21

optical and archival infrared data. Section 2 & 3 describe various data sets used in the present study. Section 4 presents short descriptions of the BRCs studied in this work. Sections 5 describes methodology to identify and characterize the YSO population of the BRCs using near-far infrared photometry. Sections 6 & 7 describe the determination of various physical parameters of the YSOs based on the colour-magnitude diagrams as well as SED fitting and star formation scenario in the studied BRCs. In section 8 we outlined the main results of the present work.

2 OBSERVATIONS AND DATA REDUCTIONS

The BVI_c observations of BRC 5, 7 and 39 were obtained using 2048×2048 pixel² CCD camera mounted at the f/13 Cassegrain focus of the 1.04-m Sampurnanand Telescope (ST) of the Aryabhata Research Institute of Observational Sciences (ARIES), Nainital, India. The details of the CCD camera can be found in our earlier paper (e.g. Jose et al. 2008, Pandey et al. 2008). To improve the signal to noise ratio, the observations were carried out in a binning mode of 2×2 pixels. During the observations the seeing was $\sim 2''$. The SA98 field of Landolt (1992) was observed on 2006, October 26 to standardize the observations of BRC 5 and BRC39. The observations of BRC 7 were standardized on 2009 October 13 by observing the standard stars in the SA92 field. Deep observations of BRC39 were carried out using the 2-m Himalayan Chandra Telescope (HCT) on 2008 October 21. The log of the HCT and ST observations is tabulated in Table 1. Bias and twilight flat frames were also taken during the observing runs.

The pre-processing of the data frames was done using the various tasks available under the *IRAF* data reduction software package. The photometric measurements of the stars were performed using *DAOPHOT – II* software package (Stetson 1987). The point spread function was obtained for each frame using several uncontaminated stars.

The instrumental magnitudes were converted to the standard values using a least-square linear regression procedure as outlined by Stetson (1992). The photometric calibration equa-

tions used are as follows:

$$v = V + (5.088 \pm 0.006) + (0.188 \pm 0.011) X + (0.032 \pm 0.007)(V - I),$$

$$i = I + (5.320 \pm 0.012) + (0.121 \pm 0.019) X + (0.106 \pm 0.011)(V - I),$$

where V and I are the standard magnitudes; v and i are the instrumental magnitudes obtained after time and aperture corrections, and X is the airmass. We have ignored the second-order colour correction terms as they are generally small in comparison to other errors present in the photometric data reduction.

The standard deviations of the standardization residuals, Δ , between the standard and transformed magnitudes and colours of the standard stars, are found to be $\Delta V = 0.01$ and $\Delta(V - I_c) = 0.01$. The photometric accuracies depend on the brightness of the stars, and the typical DAOPHOT errors in V and I_c bands at $V \sim 18$ are smaller than 0.01 mag. Near the limiting magnitude of $V \sim 21$, which is practically the same for HCT and ST, the DAOPHOT errors increase to 0.05, 0.02 mag in the V and I_c bands, respectively.

3 ARCHIVE DATA

3.1 Near-infrared data from 2MASS

NIR JHK_s data for the stars in the BRC regions have been obtained from the Two Micron All Sky Survey (2MASS) Point Source Catalog (PSC) (Cutri et al. 2003). Sources having uncertainty ≤ 0.108 mag ($S/N \geq 10$) in all the three bands were selected to ensure high quality data. The JHK_s data were transformed from the 2MASS system to the CIT system using the relations given in the 2MASS website ¹.

3.2 Mid Infrared data from Spitzer-IRAC

We have used the mid-infrared (MIR) data from the *Spitzer* Archive for BRC 5, 7 and 39. The images were obtained from the *Spitzer* archive using the software Leopard. These images were the part of program ‘‘GLIMPSE360: Completing the Spitzer Galactic Plane Survey with Infrared Array Camera (IRAC)’’ (PI: B.A. Whitney). Since BRCs 5, 7 and 39 were observed during the *Spitzer* Warm Mission, only the 3.6 μm and 4.5 μm observations were available. The images were taken in 12s High Dynamical Range mode. Standard corrected basic Calibrated Data (CBCD) products from version S18.14.0 of the *Spitzer Science*

¹ <http://www.astro.caltech.edu/~jmc/2mass/v3/transformations/>

Center's IRAC pipeline were used to make the final mosaics. Both short (0.6 s) and long (12 s) integration CBCDs frames in each channel were processed and mosaicked using MOPEX. We have processed and mosaicked the long exposures and short exposures separately. All of the mosaics were built at the native instrument resolution of $1''.2/\text{pixel}$. We used the MOPEX - APEX to detect the point sources and perform the aperture photometry on the mosaicked images in each IRAC band, as better point-response-function images were not available for *Spitzer* warm mission data. The detections were also examined visually in each band to remove non-stellar objects and false detections. In addition to this we also included manually the point sources which were not detected by APEX. We supplied the list of those sources to Apex- User list pipeline and performed the aperture photometry for those sources. The photometry was done using an aperture radius of $2''.4$ and the background estimation was done within a concentric sky annulus of the inner and outer radii of $2''.4$ and $7''.2$, respectively. The corresponding aperture corrections were applied as given in the IRAC data handbook. To convert the flux densities to magnitudes, we used the zero points as provided in the IRAC instrument Handbook. Sources with photometric uncertainties ≤ 0.2 mag in each band were considered as good detections. We made a catalogue for each channel from the short and the long exposures separately and then looked for the closest match within $1''.2$ to obtain the final catalogue of the sources obtained in both IRAC bands.

3.3 Wide-field infra-red survey Explorer data

The Wide-field Infrared Survey Explorer (WISE) has been uncovering population of YSOs embedded in dense clouds. It has been mapping the sky in four wavebands (3.4, 4.6, 12, and $22\ \mu\text{m}$) often referred to as W1, W2, W3, and W4, which are particularly useful for the characterization of star-forming regions. We have used the WISE preliminary release catalog from Cutri et al. (2012). The spatial resolution at W1, W2 and W3 is $6''$ and is $12''$ at $22\ \mu\text{m}$. We rejected any source with magnitude uncertainty > 0.2 and confusion flags (cc-flags in the catalog) that include any of “D”, “H”, “O” or “P” in W1, W2 or W3 bands.

4 NOTES ON INDIVIDUAL BRC REGIONS

Fig. 1 shows the DSS2-R band, 2MASS- K_s band and IRAC [4.5] colour-composite images of BRCs 5, 7 and 39. A brief description of each BRC region studied in the present work is given below.

BRC 5 : BRC 5 is located on the west rim of the HII region IC 1805 (also known as Sharpless S190). The bright rim of BRC 5 points towards massive stars of the cluster IC 1805 (or Melotte 15 or ocl 352) located at the center of the HII region. The distance and age estimates for the cluster varies from 1.9 to 2.4 kpc and 2 to 5 Myr, respectively (Johnson et al. 1961, Becker 1963, Joshi & Sagar 1983, Sung & Lee 1995). BRC 5 shows the signatures of recent star formation as it harbours a luminous IRAS 02252+6120 of far-infrared (FIR) luminosity $\sim 3300L_{\odot}$ (Sugitani et al. 2000; Lefloch, Lazareff & Castets 1997), which is the exciting source of the tiny, jet-like HH object (HH 586). Slitless H α emission survey by Ogura et al. (2002) revealed many H α emission stars in the region. Xiang & Turner (1995) detected water maser emission towards BRC 5, while it could not be detected by Valdetaro et al. (2005), perhaps because of the episodic nature of the water maser emission. Submillimeter observations indicates the presence of a dense core at the head (02:29:02.2, +61:33:33) of the BRC 5 (Morgan et al. 2008). The location of the IRAS source (cross symbol) and submm core (open circle) is shown in Fig. 1. White contour from NVSS 1.4 GHz continuum image traces the location of the ionised boundary layer (IBL).

BRC 7 : BRC 7 is a large cometary cloud with a broad tail, associated with the HII region IC1805. Hence, both BRC 5 and BRC 7 are located in the same H II region and irradiated by the UV flux from the massive members of IC 1805. Three of the nine O stars account for 90% of the ionizing photons. These are HD 15558 (spectral type O4 IIIf), HD 15570 (O4 If), and HD 15629 (O5 V) (Massey et al. 1995). The presence of an IRAS point source IRAS 02310+6133 of FIR luminosity of $\sim 910 L_{\odot}$ at the focus of BRC 7, where the molecular gas density reaches $\sim 10^4 \text{ cm}^{-3}$, indicates the presence of embedded star formation. Wu et al. (2004) reported a CO outflow with a dynamical age of $\sim 51.5 \times 10^4$ yr. Valdetaro et al. (2005, 2008) reported non-detection of maser emission towards BRC 7; however it was detected by Wouterloot, Brand & Fiegle (1993). Submillimeter observations of BRC 7 at 450 and 850 μm revealed a dense core at the head of the cloud. The location of the IRAS source (cross symbol) and the submm core (open circle) in BRC 7 is shown in Fig. 1. **BRC 39 :** BRC 39 is associated with the relatively old HII region IC 1396, which is excited by the massive members of the cluster Trumpler 37 (Tr 37). The age of Tr 37 is estimated as $\sim 3\text{-}5$ Myr **and is located at the distance of ~ 870 pc** (Contreras et al. 2002). This region has a rich population of BRCs including BRCs 32-42 (SFO91), among which BRCs 37 and 38 have been studied (see, e.g., Getman et al 2007, Ikeda et al. 2008). In Paper I and Paper II, we reported quantitative evidence for S^4F in BRC 37 and BRC

38, respectively. BRC 39 with an elephant trunk morphology, is also known as IC1396 E. It hosts an embedded IRAS source, IRAS 21445+5712 **with an FIR luminosity $\sim 96 L_{\odot}$** (Sugitani et al. 1991) located near the center of the BRC, but no IRAS source was found at the head like other BRCs. Ogura et al. (2002) carried out the slitless $H\alpha$ survey of BRC 39 and identified four $H\alpha$ emission stars. However, they did not find any concentration of $H\alpha$ stars in this region but noticed a small reflection nebula at the ‘apex’ of bright rim. Recently, Nakano et al. (2012) surveyed the whole IC 1396 region for $H\alpha$ emission stars, and pointed out several clusterings of $H\alpha$ stars in the region including BRC 39. Valdetaro et al. (2005) have reported water maser emission towards the BRC, which indicates the presence of YSO. Froebrich et al. (2005) detected two bright bow shocks, **HH 865 A and HH 865 B**, emerging from IRAS 21445+5712, heading to the north-west of the BRC. **The submillimeter observations by Morgan et al. (2008) at 450 and 850 μm , revealed that this BRC harbours two dense submillimeter cores, BRC39 SMM1 (21:46:01.2, +57:27:42) and BRC39 SMM2 (21:46:06.9, +57:26:36); one of which is at the head of the BRC and other at the middle. In Fig. 1, we have shown the location of the IRAS source with a cross symbol and the submm cores with open circles.**

5 IDENTIFICATION OF PRE-MAIN-SEQUENCE STARS

Since these BRCs are at low Galactic latitudes, they may be significantly contaminated by foreground/background stars. To characterize the YSO population and study the star formation scenario in BRCs, it is necessary to identify the probable associated members. Here, in the present work we used the photometric criteria to select probable members. The procedure is described below.

5.1 $H\alpha$ emission and Near infrared excess

The spectra of some pre-main sequence (PMS) stars show emission lines, among which usually $H\alpha$ is the strongest. The $H\alpha$ emission in the weak-line T-Tauri stars (WTTs) is believed to originate due to chromospheric activity and in classical T-Tauri stars (CTTs) due to magnetospheric accretion shocks. Therefore, the detection of $H\alpha$ emission stars is a powerful method to search for PMS candidates. In the present work, we used the catalog of $H\alpha$ emission stars by Ogura et al. (2002) and Nakano et al. (2012).

PMS stars also exhibit excess emission in near-infrared wavelengths due to their circumstellar disks. Hence, NIR photometric surveys of star forming regions are capable of detecting associated low-mass PMS stars associated. To identify NIR excess stars, we used NIR $(J - H)/(H - K)$ colour-colour (NIR-CC) diagram. Fig. 2 shows the NIR-CC diagrams for the studied BRCs. The thin and thick solid curves represent the unreddened main-sequence and giant branches (Bessell & Brett 1988), respectively. The dotted line indicates the locus of intrinsic CTTSs (Meyer et al. 1997). The parallel dashed lines are the reddening vectors drawn from the tip (spectral type M4) of the giant branch (“upper reddening line”), from the base (spectral type A0) of the main-sequence branch (“middle reddening line”) and from the tip of the intrinsic CTTS line (“lower reddening line”). The extinction ratios $A_J/A_V = 0.265$, $A_H/A_V = 0.155$ and $A_K/A_V = 0.090$ have been adopted from Cohen et al. (1981), with the 2MASS data and intrinsic curves all converted to the CIT system. We classified sources into three regions in the NIR-CC diagrams (for details; see Paper II). Objects falling in the ‘T’ and ‘P’ regions of NIR-CC diagrams are considered as NIR excess stars and probable members of the BRC aggregates. These sources are included in the analysis of the present study in addition to the $H\alpha$ emission stars.

5.2 YSOs from NIR/MIR photometry

Since stars inside the rim are often deeply embedded, MIR observations by the *Spitzer Space Telescope* can provide a deeper insight into the embedded YSOs. IRAC colour-colour diagrams are powerful tools to identify and classify the embedded YSOs. Gutermuth et al. (2009) have developed a procedure to identify and classify the YSOs on the basis of 2MASS and IRAC photometry. Since the [5.8] and [8.0] bands data are not available, for these regions we used the K_s , 3.6 μm and 4.5 μm band data to identify and classify the YSOs adopting the procedure given by Gutermuth et al. (2009). To implement the YSO identification, first we generated the extinction map for the regions using 2MASS data. Here, we compute stellar extinction maps with the method proposed by Cambr esy et al. (2002). This method uses adaptive cells that contain a fixed number of stars instead of cells of fixed size. If n_* is the number of stars per cell, each cell is defined by the closest n_* stars to the cell center. In this way the spatial resolution depends on the local stellar density. The spatial resolution is higher in regions of low extinction where star density is higher, than in regions of large extinction. Hence, this method may underestimate the extinction towards the region where

Table 2. YSOs from 2MASS, IRAC and WISE photometry

Id	RA (J2000)	DEC (J2000)	J±eJ	H±eH	K±eK	[3.6]± e[3.6]	[4.5]± e[4.5]	[3.4]± e[3.4]	[4.6]± e[4.6]	[12]± e[12]	[22] ±e[22]	comment
BRC5												
1	36.97895	61.54822	16.28 ± 0.10	14.73 ± 0.07	13.80 ± 0.05	-	-	12.16 ± 0.08	11.16 ± 0.056	7.74 ± 0.28	-	NIR excess
2	36.99766	61.57376	14.02 ± 0.03	12.78 ± 0.03	11.87 ± 0.02	-	-	10.78 ± 0.04	10.18 ± 0.032	-	-	"
3	37.00884	61.58534	16.50 ± 0.10	14.94 ± 0.06	13.98 ± 0.05	-	-	-	-	-	-	"
.

dense clumps or cloud fragments are present. The average spatial resolution over the whole map can be changed by adjusting the number of stars per cell.

We computed the colour excess (E), using the relation $E = (H-K_s)_{obs} - (H-K_s)_{int}$, where $(H-K_s)_{obs}$ is the observed median color in a cell and $(H-K_s)_{int}$ is the intrinsic median color, estimated from the colors of supposedly unreddened stars. The use of median color has the advantage of minimizing the effect of foreground stars. To obtain the intrinsic median colour, we selected nearby field regions which were devoid of nebulosity or any CO emission features. Visual extinction values are obtained from the color excess using the relation $A_V = 15.87 E$. We calculated A_{K_s} for each star using the relation $A_{K_s} = 1.82 E$. The colour excess ratios presented in Flaherty et al. (2007) have been used to compute the dereddened $(K-[3.6])$ and $([3.6]-[4.5])$ colours. Based on the $(K-[3.6])_0$ and $([3.6]-[4.5])_0$ colour criteria, class I and class II sources are selected. However, to remove extragalactic contaminants, we have selected objects having $[3.6] < 14.5$, where the contamination from the extra-galactic sources is expected to be less than 50%. Fig. 3 shows the 2MASS/IRAC $([3.6]-[4.5])_0 - (K_s - [3.6])_0$ colour-colour diagrams for BRC 5, BRC 7 and BRC 39 used to discriminate class II and class I systems. Using this method we identified 7 class I and 94 class II sources in BRC 5, 1 class I and 52 class II sources in BRC7, 3 class I and 23 class II sources in BRC 39.

5.3 The WISE data

In the absence of *Spitzer* longer wavelength data, we used WISE data for further detection and characterization of YSOs embedded in star forming regions. The W3 and W4, in particular, are well suited for the detection of warm circumstellar dust and objects embedded in dense material. Although infrared wavelengths can penetrate dense material and are particularly useful to unravel the sources hidden in the silhouette of dust layers, these wavelengths also become transparent to the background contaminating sources, specially for polyaromatic hydrocarbon (PAH) emitting galaxies, active galactic nuclei (AGNs) which may contaminate our YSO sample. To weed out these contaminants from the YSO sample we have used the approach developed by Koenig et al. (2012; references therein). This se-

lection method uses the series of colour and magnitude cuts to remove the contaminants such as background galaxies or nebulosity blobs. To ensure high quality data, our sample contains only those stars which have photometric error < 0.2 mag in all W1, W2 and W3 bands. Fig. 4 shows the colour-colour diagrams for the class 0/I and class II sources in BRCs 5, 7 and BRC 39 regions. We obtained 9 class I and 11 class II sources in BRC 5, 4 class I and 19 class II sources in BRC 7, 6 class I and 19 class II sources in BRC 39 regions. The spatial distribution of the class 0/I and class II sources obtained from WISE and IRAC data is shown in Fig. 5. Triangles represent the IR excess sources selected based on the NIR CC diagram. The YSOs identified and classified based on the 2MASS, IRAC and WISE colours as well as their magnitudes in different bands are tabulated in Table 2.

6 OPTICAL PROPERTIES OF THE SELECTED YSOS : COLOUR-MAGNITUDE DIAGRAM

Although we have attempted to remove the contaminants from the YSO sample using the method described in Section 5, it may still contain a few sources which are not YSOs. The ancillary data are very important for weeding the contamination out from the YSO sample. The position of YSOs, which are not deeply embedded, in the HR diagram can be used to confirm their evolutionary stages and young nature. Hence, we exploit the optical VI_c data to further characterize the census of YSOs.

To construct the colour-magnitude diagrams (CMDs) of the YSOs in the regions, it is necessary to estimate reddening. In the present study we used the NIR $(J - H)/(H - K)$ colour-colour diagram to determine the reddening. To estimate the visual extinction (A_V) value of an individual star it is traced back to the intrinsic T-Tauri locus parallel to the reddening vector. We calculated mean reddening of the YSOs in BRC regions. To construct CMDs, in case of BRCs 5/7 we have adopted a distance of $2.2 Kpc$ and for BRC 39 a distance of 870 pc (Contreras et al. 2002). Fig. 6 shows the CMDs for the YSOs in BRCs 5, 7 and 39, respectively. The post-main sequence isochrone for 4 Myr by Girardi et al. (2002), which is practically a zero-age-main sequence (ZAMS), and PMS isochrones for 1 and 5 Myr for the solar metallicity by Siess et al. (2000) are also plotted. The isochrones are shifted for the adopted distance and mean reddening of the individual BRCs.

The age and mass of each YSO given in Table 3, was estimated by referring to the isochrones and using the $V/(V - I_c)$ colour-magnitude diagrams as discussed in Pandey et al.

al. (2008) and Paper II. The ages range from 0.1 to a few Myr (with some exceptions). The estimation of the ages of the PMS stars by comparing the observations with the theoretical isochrones is prone to random errors in observations and systematic errors due to the variation among different theoretical evolutionary tracks (see e.g. Hillenbrand 2005). The effect of random errors in determination of A_V , age and mass was estimated by propagating the random errors to the observed estimation by assuming normal error distribution and using the Monte-Carlo simulations. The use of different PMS evolutionary model gives different age and age spread in a cluster (e.g. Sung et al. 2000). Here in the present study we have used model by Siess et al. (2000) only for all the BRCs, therefore our age and mass estimations do not include systematic errors. The presence of binaries may be another source of error in age determination. The presence of binary will brighten a star, consequently the CMD will yield a lower age estimate. In the case of an equal mass binary we expect an error of ~ 50 - 60% in age estimation of PMS stars. However, it is difficult to estimate the influence of binaries on mean age estimation as the fraction of binaries is not known. Here we would like to point out that we are interested mainly in the *relative* ages of the aggregate members, in particular, their spatial distribution with respect to the bright rim.

7 STAR FORMATION SCENARIO IN BRC REGIONS

7.1 Mid/Far IR view of the BRCs

Figure 5 shows the three-color composite image of BRCs 5, 7, 39 using WISE 3.4, 12 and 22 μm bands. The 3.4 μm band traces mostly the emission from the stellar photosphere. The 12 μm band emission traces regions dominated by PAH emission. These complex PAH molecules absorb far UV photons and re-emit in the IR regime at 7.7 μm and 8.6 μm , which reveals the photon dominated region (PDR) preceding the ionisation-front as the shock moves into the head of the cloud. WISE 22 μm band traces the warm dust emission from heated small dust grains. In Fig. 5, we have also overplotted the contours from the Bolocam Galactic Plane Survey (BGPS; Aguirre et al. 2011). BGPS is a 1.1 mm continuum survey of the Galactic plane using Bolocam on the Caltech Submillimeter Observatory. The BGPS images and source catalogs are available through <http://irsa.ipac.caltech.edu>.

Since protostellar cores are very cold (10-20 K), their SEDs peak at submillimeter or millimeter wavelengths. The millimeter continuum emission traces emission from the dense dust cores which may eventually form a star or stellar systems, so their presence indicates

future star forming activity in the region. The BGPS image of the IC1805 region shows that the interior HII region is devoid of any 1.1 mm emission while it is present on the western side and the north-eastern side of the HII region (towards BRCs 5 and 7). Slightly south-west of BRC 5, a filamentary distribution of some red sources (possibly YSOs) enclosed by the 1.1 mm emission contours, are seen. Since the 1.1 mm emission is related with far-infrared sources these cores may be protostellar in nature. In case of BRC 39, the position of the 1.1 mm core coincides with the location of the submm core (SMM1) observed by Morgan et al. (2008), which is near the head of the globule.

7.2 Spatial distribution of Class II and Class I YSOs

BRCs are small remnant clouds with bright ionised rims which point to the ionising star(s). The pressure driven by the propagating ionisation/shock front on the surface of the cloud overcomes the internal pressure of the clouds and may initiate star formation inside the head of the cloud. Molecular, infrared and $H\alpha$ surveys can be used to trace recent or ongoing star formation. A triggered BRC generally shows the presence of dense cores inside the head of the cloud and an aligned distribution of YSOs. Hence, the age gradients of YSOs and their aligned spatial distribution from the ionizing source are used to diagnose the working of RDI process.

BRC5 is one of the most promising BRC candidates found to be in the state of equilibrium. It is associated with an IRAS source as well as a submillimeter core (Morgan et al. 2004; 2009), indicating that this cloud is undergoing star formation. The spatial distribution of the YSOs in the region shows that the Class II sources are distributed throughout the region an-isotropically, while the Class I sources are generally located within the bright rims. YSOs identified from 2MASS/IRAC as well as WISE photometry appear to be spatially aligned. Similarly, in BRC 7, the distribution of YSOs is also non-uniform, containing many class II sources, most of which are distributed in front of the bright rim and seem to form a slightly elongated cluster. The NIR/MIR survey of the regions reveals an aligned distribution of the YSOs, and small clusters of disk bearing PMS stars within and in front of the bright rims are also clearly visible.

BRC 39 region has an elephant trunk-like morphology and contains an IRAS source in the middle of the globule. Morgan et al. (2008) found two submillimeter cores in the BRC. The spatial distribution of the YSOs shown in Figure 4 also indicates the density enhancement

Table 3. Magnitudes, Age/mass of the YSOs in the BRC regions

Id	V ± eV	I ± eI	Mass ± error in Mass (M_{\odot})	Age ± error Age(Myrs)	Flag
BRC 5					
7	20.81 ± 0.05	18.47 ± 0.02	0.91 ± 0.01	> 5	
10	22.51 ± 0.13	18.85 ± 0.07	0.31 ± 0.02	1.72 ± 0.28	
11	20.08 ± 0.02	17.64 ± 0.01	1.17 ± 0.01	> 5	
...

near the head of the globule. Additionally, we also notice the loose clustering of YSOs southward of BRC 39, which is designated as BRC 41 in the SFO91 catalogue. Recently Morgan et al. (2009) refined the SFO 91 catalogue and based on the observation criteria they have classified BRCs into triggered and non-triggered samples using three criteria: presence of the IBL, presence of MSX emission (to trace the PDR) and presence of submillimeter cores. To establish the presence of IBL, they have used the 21 cm emission feature from the NVSS survey. Although BRC 39 shows the presence of MSX emission and contains two submm cores, the 21 cm emission feature was not above the 3σ level, so it is rejected as the case of triggered star formation.

7.3 Evolutionary stages of YSOs from SED fitting

To ascertain the young nature of the YSOs identified from the photometric observations, we modeled their spectral energy distributions (SEDs) using the fitting tools of Robitaille et al. (2006, 2007). The models are computed using a Monte-Carlo-based radiation transfer code (Whitney et al. 2003a, 2003b), which use combinations of the parameters of the central star, accreting disk, infalling envelope and bipolar cavity. Although interpreting SEDs using the radiative transfer code is subject to degeneracies, the spatially resolved multiwavelength observations can often break the degeneracy. In the present work, to constrain the parameters of the stellar photosphere and circumstellar environment, we fit the SEDs to only those sources for which we have fluxes at 12 μm or longer wavelengths. We looked for the counterparts of the identified YSOs in the 2MASS Point Source Catalog (Cutri et al. 2003), WISE catalog, optical (V,I) / PANSTARR (g, r, i, z).

As stated in Robitaille (2008), the SED fitting tool deals with a single source, and input fluxes from multiple sources in a beam can result in incorrect stellar age and mass. Similarly, any erroneous fluxes can seriously affect the chances of obtaining a sensible SED and thus sensible physical parameters. Since IRAC has a higher spatial resolution than WISE, wherever available, we preferred the IRAC 3.6 μm and 4.5 μm fluxes. Similarly, we

used only fluxes at 12 μm and 22 μm as inputs that have good quality-flags and errors ≤ 0.2 mag.

The SED-fitting tool fits each of the models to the data, allowing the distance and interstellar extinction to be free parameters. In case of BRCs 5 & 7, we have assumed the distance range from 1.9 to 2.2 kpc and in the case of BRC 39 from 0.75 to 0.87 kpc. Since we do not have spectral-type information for our identified YSOs, in order to derive their approximate extinction values, we traced back these sources along the reddening vector to the intrinsic late MS locus or its extension in the NIR CC diagram. Considering the uncertainties that might have gone into the estimates, we used the estimated value $A_V \pm 2.5$ mag as an input parameter for these sources. For Class I sources, for which we do not have NIR data, we allow A_V up to 25 mag. We further set 10% to 30% error in the flux estimates due to possible uncertainties in the calibration and intrinsic object variability. Figure 7 shows examples of the SEDs and the resulting models for Class II and Class I sources. We obtained physical parameters for all the sources adopting an approach similar to that of Robitaille et al. (2007) by considering those models that satisfy

$$\chi^2 - \chi_{\min}^2 \leq 2N_{\text{data}},$$

where χ_{\min}^2 is the goodness-of-fit parameter for the best-fit model and N_{data} is the number of input observational data points. The parameters are obtained from the weighted mean and the standard deviation of these models, weighted by $e^{(-\chi^2/2)}$ of each model, and are shown in Table 4. These parameters are obtained from the set of models that represent the overall distribution and therefore more likely suppress any extreme values that may arise due to a few badly fitted models. However, due to limited observational data points, some of the parameters from the model fits can be narrowly constrained over others depending on the available fluxes. Table 4 lists the Id, χ_{\min}^2 , star mass (M_{\star}), temperature (T_{\star}), stellar age (t_{\star}), mass of the disk (M_{disk}), disk accretion rate (\dot{M}_{disk}), foreground visual absorption (A_V), the of the best fit, and the number of data points (N_{data}). However, it is worthwhile mentioning that due to the lack of the fluxes at optical wavelengths, the age and mass of these class 0/I sources are less constrained. In the Robitaille et al. (2007) models, the stellar masses and ages are sampled using the isochrones and evolutionary tracks (Bernasconi & Maeder 1996; Siess et al. 2000) from the stellar luminosity and temperature, derived from the SED models. Since the age determination for all the YSOs is being made following the same set of evolutionary tracks, we therefore use the relative age among the YSOs to constrain the star

Table 4. Physical parameters of the YSOs obtained from SED fits

ID	χ^2_{min}	M_* (M_\odot)	T_* (10^3 K)	t_* (10^6 yr)	M_{disk} (M_\odot)	\dot{M}_{disk} ($10^{-8} M_\odot/\text{yr}$)	A_V mag	N_{data}
BRC 5								
1	3.47	2.7 ± 1.3	4.4 ± 0.6	0.2 ± 0.1	0.018 ± 0.036	31.005 ± 29.257	6.5 ± 1.4	10
16	35.03	1.4 ± 0.9	4.4 ± 0.6	0.7 ± 0.9	0.003 ± 0.003	1.108 ± 1.108	2.5 ± 0.4	11
24	3.45	1.4 ± 0.8	4.4 ± 0.4	2.3 ± 1.7	0.011 ± 0.013	4.733 ± 4.397	4.6 ± 1.0	8
...

formation history of the complex. However, we are aware of the fact that the age estimation depends on the choice of isochrones. For example, Hillenbrand et al. (2008) suggested that the use of a different set of isochrones can lead to a systematic uncertainty at a level of 0.75 dex for sub-solar mass stars, though the agreement is better for older PMS solar mass stars. The age estimation for an accreting embedded protostar is highly uncertain and so should be considered as a quantitative indicator of stellar youth.

We note that BRC 39, all of the YSOs have ages < 7 Myr. One of the IRAC sources (Id:....), which is at the head of the cloud, but was detected only in IRAC images, coincides with the position of the submillimeter core detected by Morgan et al. (2008). We have considered the IRAC fluxes along with WISE, 450 μm and 850 μm data for this particular star. The SED fitting yields an age of 8×10^4 yr, which is comparable to the lifetime of a class 0 system. The class 0/I source (Id...)obtained from the WISE photometry in BRC 5 also has counterparts at 450 and 850 μm wavelength. The SED fitting of the fluxes from 3.4 to 850 μm suggests that it is a massive star ($\sim 11 M_\odot$) and age few 10^4 year. A CO outflow, with a dynamical age of $\sim 1.5 \times 10^4$ yr, has been detected in the direction of the head of the globule (Duvert et al. 1990, Lefloch, Lazareff & Castets 1997). The age of the massive star is comparable to the dynamical age of the outflow.

In case of BRC 7, a class 0/I source (ID ...) just inside the bright rim, has no 2MASS counterparts and coincides with the submillimeter core from Morgan et al. (2008). The SED fitting from 2.1 to 850 μm yields a mass of $\sim 6 M_\odot$ and age of $\sim 10^4$ years, which is comparable to the age of the outflow.

7.4 Small-Scale Sequential Star Formation (S^4F)

As for the S^4F hypothesis on the RDI star formation, there has been only qualitative evidence such as an asymmetric spatial distribution of probable TTSs (Ogura et al. 2002). Very recently Paper I and Paper II have quantitatively verified the S^4F hypothesis by using

Table 5. Mean age of the YSOs inside and outside a bright rim

Region	Inside/on bright rim Mean age (Myr) (No. of stars)	Outside bright rim Mean age (Myr) (No. of stars)
BRC 5	1.76 ± 1.17 (19)	2.06 ± 1.24 (17)
BRC 7	0.91 ± 0.71 (13)	1.38 ± 0.77 (25)

BVI_c photometry of four BRCs. In the present study we follow the same approach as given in Paper I and II. We have divided the YSOs ($H\alpha$ stars, IR excess stars, IRAC and WISE YSOs) associated with BRCs into two groups: those lying on/inside versus outside of the rims. Mean ages have been calculated. There are a few stars in Table 3 with inferred ages older than 5 Myr. Since the maximum ages of the associated ionizing sources of BRCs studied here are ~ 5 Myr, therefore the YSOs having ages greater than 5 Myr can not be expected as products of triggered star formation. We suspect that they may have formed in the original molecular cloud prior to the formation of the HII regions or some of them may be field stars, thus their positions in the CMDs yield the higher ages. When calculating the mean ages we have not included those stars. The results are given in Table 5, which shows that the mean age of the YSOs lying on/inside the rim is younger than those located outside.

The above results are the same as those obtained in Paper I and II. Therefore, the present results further confirm the S^4F hypothesis. However, scatter in the stellar ages for each region of all BRCs in spite of a clear trend of the mean ages, can be observed. Possible reasons for the scatter include photometric errors, errors in extinction correction, light variation of young stars, their proper motions, and binarity, etc. As discussed in Paper I, photometric errors, light variation and extinction correction do not seem to be the major reason for the scatter. However, the proper motions of newly born stars may be the main cause of the scatter.

7.5 Indication of Global Triggered Star Formation

BRCs are considered to be remnants originated from dense parts (cores) in an inhomogeneous giant molecular cloud. If the original cloud was big enough, the resultant BRC could have undergone a series of RDI events, leaving an elongated distribution of young stars. The distribution of such YSOs and its morphological details could be used to probe the star formation history in the OB association. Both BRC 5 and BRC 7 show the observational features of RDI triggered star formation by the ultraviolet radiation from the massive member(s) in IC 1805 or Melotte 15. Both of these BRCs possess IRAS sources inside their

rim. Fig. 5 shows the spatial distribution of young stars identified from 2MASS, IRAC and WISE photometry in BRCs 5, 7 and 39. We can observe that most of the class II sources are widely distributed and mostly class I sources are inside the clouds. The spatial gradient of evolutionary stages of YSOs, i.e., presence of class I sources, submm/mm cores inside the BRCs as well as aligned distribution of YSOs from the massive star(s) indicates that the radiation pressure is efficiently affecting the star formation in the regions. BRCs 5 and 7 both possess small clusters of YSOs, which in case of BRC 7 is more prominent and more exposed. This cluster is visible in 2MASS K_s as well as IRAC and WISE images. The close proximity to the rim and the young nature of the stellar members indicate young cluster. However, this cluster is not associated with nebulosity; the gas in this region has likely been dispersed by winds and radiation from massive members of the cluster IC1805. Its formation may be the result of the implosion of original cloud which is now moved slowly due to the photo-evaporation of the globule material. The slightly elongated morphology of the cluster further strengthens the idea. We examined the elongation of the cluster, distribution of IR excess sources as well as class 0/I/II sources obtained from the IRAC/WISE photometry and the axis symmetry of the cloud. The direction from the mean position of the three most massive stars, HD 15570, HD 15558, HD 15629 to the IRAS source (marked as in Fig. 5) is nearly parallel to the elongation direction of the axis of the BRC. It suggests that the cloud has been strongly affected by the UV radiation from these stars. However, the distribution of the class II sources has a different elongation direction, almost aligned along a line, whose direction differs from that of the UV radiation from these three massive stars. The elongated distribution of the young stars points to the direction of an O6 V star (BD +60 497). If the YSO alignment and the elongation of the cluster were originally made under the influence of BD +60 497, its impact might have been dominant before the other exciting star(s) became dominant. This suggests that the main exciting stars were born quite recently compared to the O6 V star. The directions almost agree with each other, which indicates that these YSOs have been formed due to the strong UV impact of the main exciting stars (HD 15570, HD 15558, HD 15629) and/or the O6 V star. Also the presence of millimeter cores and 21 cm continuum emission at the west side of the cloud (see Fig. 1b) indicates that it is more exposed to the UV radiation from the western side. The morphology of the tip of the rim also supports the idea. T Since BRC 5 is also located in the same HII region and its evolution is subjected by the same ionising stars, we also examined the possible role of BD +60 497 on the evolution of the cloud. Lefloch, Lazareff & Castet (1997) using molecular and

continuum observations compared the distribution of ionised gas along the cloud rim and the general symmetry of the cloud. They suggested that the cloud acquired its shape in a previous episode of photo-evaporation by now-extincted stars and it is presently undergoing re-compression from the south side by the O star cluster located at the center of the HII region. The O6 V star is nearly aligned with the apex of BRC 5 and thus most likely source responsible for the current morphology of BRC 5.

In case of BRC 5 the mean age of the cluster members of IC 1805 as ~ 4 Myr whereas the mean age of the YSOs outside the bright rim is ~ 2.1 Myr and ~ 1.8 Myr inside/on it. This is an evidence of age gradient. Similarly, In case of BRC 7 the stellar ages also decreases from 4 Myr of the central cluster, to 1.4 Myr outside the rim, to ~ 0.9 Myr inside/on the rim and provide evidence for the RDI triggered star formation in the region. The

In case of BRC 39 the DSS2-R band image shows that the symmetry axis of the BRC as well as the curvature of the rim do not point to the most massive star (O6.5V) HD 206267 (see fig 5c of the region). To explore the possibility of other ionising star(s) which may influence the geometry and evolution of the cloud, we searched for other massive stars (earlier than B2) in the region in the SIMBAD database. We found a B0 V star, HD 206773, member of Tr 37, to be the closest massive star to the BRC and aligned with the apex of the cloud. The distance of the apex of the cloud from HD 206773 is nearly half of that from the main exciting source, HD 206267. However, considering the total output flux and distance of these two stars, the contribution of the ionising radiation from HD 206773 is only 21% of the total as compared to the HD 206267, so on the large scale the morphology of the cloud may be primarily influenced by the O6.5 V star, whereas on smaller scale B0 star might have played dominant role. Based on the optical CMD, we found an older age for a star at the middle of the globule. This star coincides with the H α star no. 3 of Ogura et al. (2002) and an IRAS source for which Voldettaro et al. (2005) detected water maser emission. But Voldettaro et al. (2005) suggested that the star in the middle is a foreground star, so not related to the globule. The adaptive optics observations of the globule by Connelley et al. (2009) suggested a possible companion at $0''.69$ separation. Hence, it may be possible that excess emission in infrared wavelengths is from the optically faint, embedded star.

Figure 4(c) also shows the intricate structure in the region with globules smaller than the BRC and pointing towards massive stars. These small globules generally show the presence of stars at their tips. The IRAC/WISE photometry of the stars at the tips indicates class I/class II sources, confirming their early state of evolution. These are morphologically similar

to the elephant trunk like structure stars (ETLSs) found in W5 E HII region (Chauhan et al. 2011b). Hence, we propose that both RDI and dynamical instability are possibly working in the region. Although BRC 39 is excluded from the sample of the triggered BRCs (Morgan et al. 2009) association with the IRAS source, H α emission stars, many class I/II sources & submm/mm cores shows that BRC 39 is an active site of star formation.

8 CONCLUSIONS

On the basis of the present optical and IR analysis of three BRC aggregates we reached the following conclusions. The presence of exciting star(s) and a molecular cloud surrounded by an ionized rim facing the exciting stars, a dense molecular core close to the rim and the spatial distribution of young stars oriented toward the exciting star(s) confirm the significant role of massive stars on the star formation activity and evolution of the BRCs. All of the BRCs contain small grouping of young stars at the head, or just outside, which favours the idea that triggering due to RDI from massive stars is giving birth to the second generation star clusters/groups. In the case of BRC 7, we found a group of mainly class II sources at the front of the rim which may be the final product of the implosion of a big massive cloud fragment. The mean age of the YSOs inside the rim is found to be less than that of the YSOs outside, which further confirms the scenario of small scale sequential star formation in BRC 5 and BRC7. We also found small ETLSs in the BRC 39 region and these ETLSs contains stars at their tips which are at the early stage of evolution suggesting that both RDI and hydrodynamical instability are working in the region.

9 ACKNOWLEDGMENTS

This publication makes use of data from the Two Micron All Sky Survey (a joint project of the University of Massachusetts and the Infrared Processing and Analysis Center/ California Institute of Technology, funded by the National Aeronautics and Space Administration and the National Science Foundation), archival data obtained with the *Spitzer Space Telescope* (operated by the Jet Propulsion Laboratory, California Institute of Technology, under contract with the NASA) and archival data obtained from the Wide Infrared Survey Explorer (WISE).

REFERENCES

- Aguirre J.E., Ginsburg A.G., Dunham M.K., Drosback M.M., Bally J. et al. 2011, *ApJS*, 192, 4
- Becker W. 1963, *ZA*, 57, 117
- Bertoldi F., 1989, *ApJ*, 346, 735
- Bessell M.S., & Brett J.M. 1988, *PASP*, 100, 1134
- Cambr esy L., Beichman C. A., Jarrett T. H., Cutri R. M 2002, *AJ*, 123, 2559
- Chauhan N., Ogura K., Pandey A. K., Samal M. R., & Bhatt B. C. 2011b, *PASJ*, 63, 795
- Chauhan N., Pandey A. K., Ogura K., Ojha D. K., Bhatt B. C., Ghosh S. K., Rawat P. S. 2009, *MNRAS*, 396, 964 (Paper II)
- Cohen J.G., Frogel J.A., Persson S.E., & Elias J.H. 1981, *ApJ*, 249, 481
- Connelley M. S.; Reipurth B.; Tokunaga A. T. 2009, *AJ*, 138, 1193
- Contreras Maria E., Sicilia-Aguilar A., Muzerolle J., Calvet N., Berlind P., Hartmann L., 2002, *ApJ*, 124, 1585
- Cutri R.M., Skrutskie M.F., Van Dyk S. et al. 2003, *Vizie Online Data Catalog*, 2246, O
- Deharveng L., Zavagno A., Caplan J. 2005, *A&A*, 433, 565
- Duvert G., Cernicharo J., Bachiller R., Gomez-Gonzalez J. 1990, 233, 190
- Elmegreen B.G., & Lada C.J. 1977, *ApJ*, 214, 725
- Froebrich D., Scholz A., Eisl offel J., & Murphy C. C. 2005, *A&A*, 432, 575
- Getman K.V., Feigelson E.D., Garmire G., Broos P., & Wang J. 2007, *ApJ*, 654, 316
- Girardi L., Bertelli G., Bressan A., Chiosi C., Groenewegen M.A.T., et al. 2002, *A&A*, 391,195
- Gutermuth R. A., Megeath S. T., Myers P. C., Allen L. E., Pipher J. L., Fazio G. G 2009, *ApJS*, 184,18
- Hillenbrand L.A., Strom S.E., Vrba F.J., Keene J. 1992, *ApJ*, 397, 613
- Ikedo H., Sugitani, K., Watanabe M. et al. 2008, *AJ*, 135, 2323
- Johnson H. L., Hoag A. A., Iriarte B., Mitchell R. I., Hallam K. L. 1961, *LowOB*, 5, 133
- Jose J., Pandey A.K., Ojha D.K., Ogura K., Chen W.P., Bhatt B.C., Ghosh S.K., Mito H., Maheswar G., Sharma S. 2008, *MNRAS*, 384, 1675
- Joshi U. C. & Sagar R. 1983, *JRASC*, 77, 40
- Kessel-Deynet O., & Burkert A. 2003, *MNRAS*, 338, 545
- Koenig X. P., Leisawitz D. T., Benford D. J., Rebull L. M., Padgett D. L., Assef R. J.

2012, ApJ, 744, 130

Landolt A.U. 1992, AJ, 104, 340

Lee H.T., Chen W.P., Zhang Z.W., Hu J.Y. 2005, ApJ, 624, 808

Lefloch B., Lazareff B. 1995, A&A, 301, 522

Lefloch B., Lazareff B., Castets A. 1997, A&A, 324, 249

Massey P., Johnson K. E., Degioia-Eastwood K. 1995, ApJ, 454, 151

Meyer M., Calvet N., & Hillenbrand, L. A. 1997, AJ, 114, 288

Morgan L.K., Thompson M.A., Urquhart J.S., White G.J., Mio J. 2004, A&A, 426, 535

Morgan L.K., Thompson M.A., Urquhart J.S., White G.J. 2008, A&A,

Morgan L.K., Urquhart J.S., Thompson M.A. 2009, MNRAS, 400,1726

Nakano M., Sugitani K., Watanabe M., Fukuda N., Ishihara D., Ueno M. 2012, AJ, 143, 61

Normandeau M., Taylor A. R., Dewdney P. E. 1996, Nature, 380, 687

Ogura K., Sugitani K., Pickles A. 2002, AJ, 123, 2597

Ogura K., Chauhan N., Pandey A.K., Bhatt B.C., Ojha D.K., Itoh Y. 2007, PASJ, 59, 199 (Paper I)

Pandey A.K., Sharma S., Ogura K., Ojha D.K., Chen W.P., Bhatt B.C., Ghosh S.K. 2008, MNRAS, 383,1241

Reach, W. et al., 2006, Infrared Array Camera Data Handbook, version 3.0, Spitzer Science Centre, California Institute of Technology, Pasadena, California 91125 USA

Robitaille T. P., Whitney B. A., Indebetouw R., & Wood K. 2007, ApJS, 169, 328

Sharma S., Pandey A.K., Ojha D.K., Chen W.P., Ghosh S.K., Bhatt B.C., Maheswar G., Sagar R. 2007, MNRAS, 380, 1141

Siess L., Dufour E., Forestini M. 2000, A&A, 358, 593

Stetson P.B. 1987, PASP, 99, 191

Sugitani K., Fukui Y., Ogura K. 1991, ApJS, 77, 59 (SFO91)

Sugitani K., Ogura K. 1994, ApJS, 92, 163

Sugitani K., Tamura M., Ogura K. 1995, ApJ, 455, L39

Sugitani K., Matsuo H., Nakano M., Tamura M., Ogura K. 2000, AJ, 119, 323

Sung H. & Lee S.-W. 1995, JKAS, 28, 119

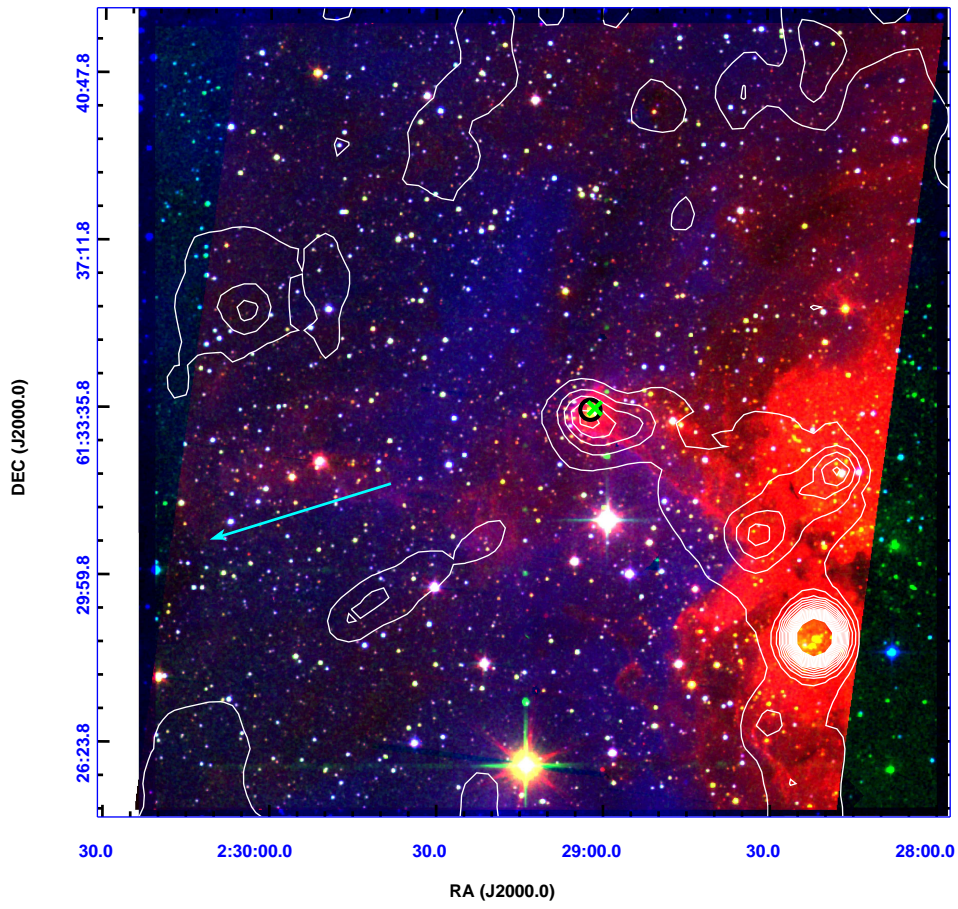
Sung H., Chun M. Y., Bessel M.S. 2000, AJ, 120, 333

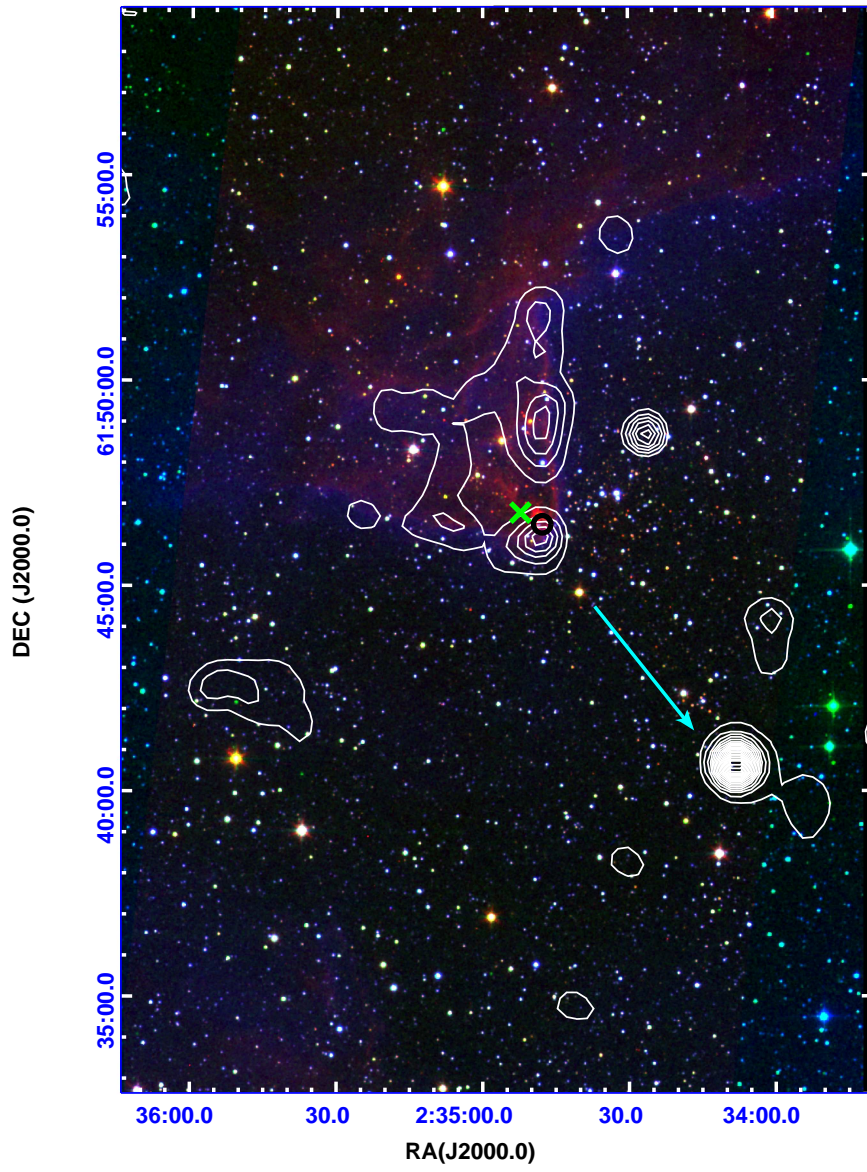
Taylor A. R., Irwin J. A., Matthews H. E.; Heyer M. H. 1999, ApJ, 513, 339

Valdettaro R., Migenes V., Trinidad M. A., Brand J., Palla F. 2008, ApJ, 675, 1352

- Valdettaro R., Palla F., Brand J., & Cesaroni R. 2005, *A&A*, 443, 535
- Whitney B. A., Wood K., Bjorkman J. E., & Cohen M. 2003a, *ApJ*, 598, 1079
- Whitney B. A., Wood K., Bjorkman J. E., & Wolff M. J. 2003b, *ApJ*, 591, 1049
- Wouterloot J. G. A., Brand J. & Fiegle K. 1993, *A&AS*, 98, 589
- Wu Y., Wei Y., Zhao M., Shi Y., Yu W., Qin S., Huang M. 2004, *A&A*, 426, 503
- Xiang D. & Turner B. E. 1995, *ApJS*, 99, 121

This paper has been typeset from a \TeX / \LaTeX file prepared by the author.





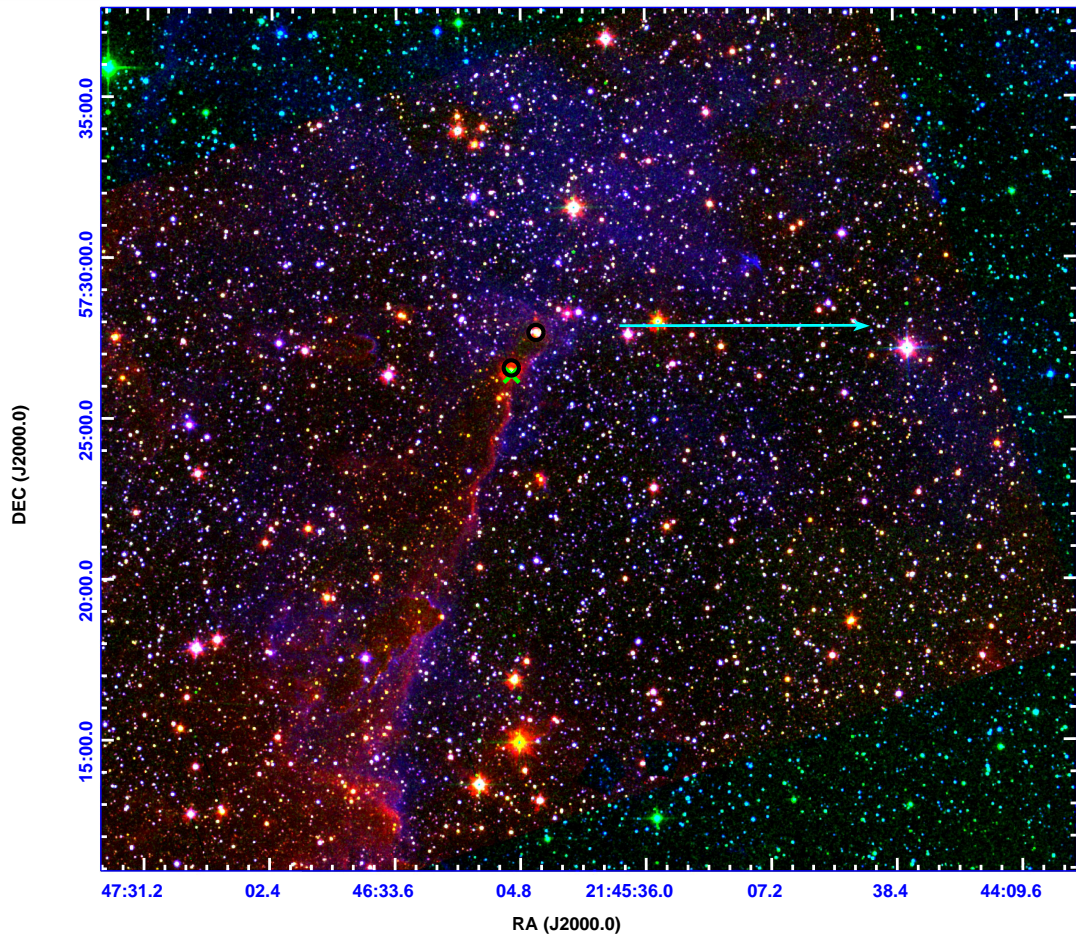


Figure 1. DSS2-R (blue), 2MASS-Ks(green) and IRAC 4.5 μm (red) colour-composite image of BRCs 5, 7 and 39. Open circles represent the location of the submm cores and cross represents the IRAS sources. Contours represents the 1.4 GHz continuum emission from the NVSS images. Vector shows the direction of ionizing star(s) mentioned in literature.

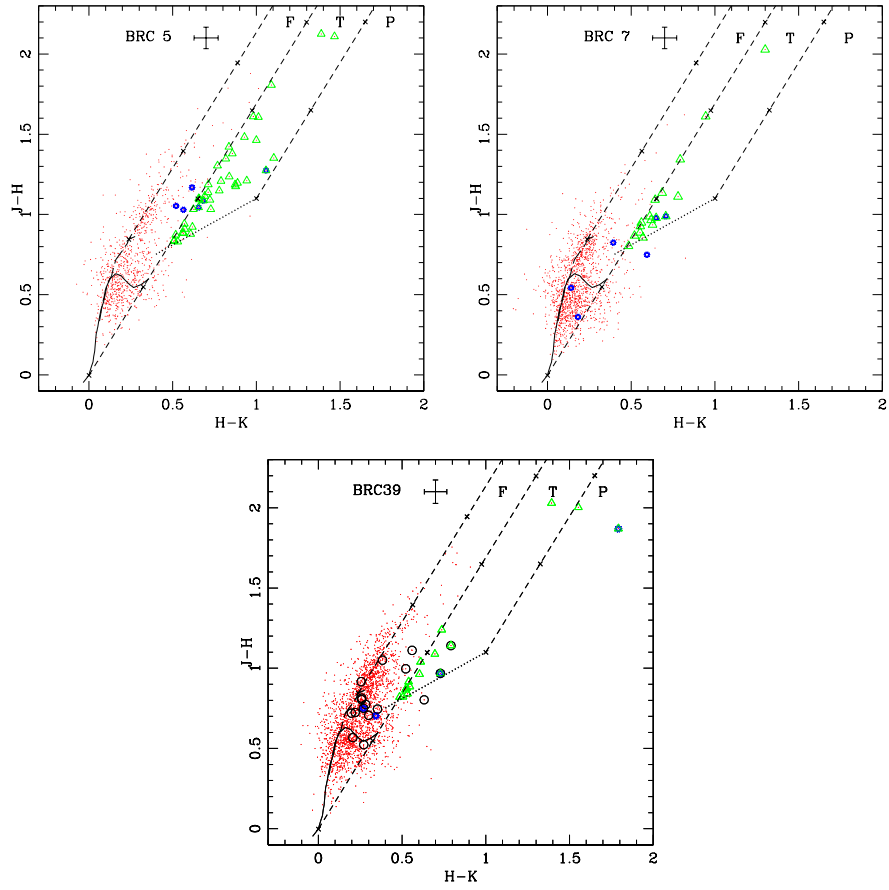


Figure 2. $(J - H)/(H - K)$ colour-colour diagrams for (a) BRC 5, (b) BRC 7 and (c) BRC 39. Magenta circles represent NIR excess stars, blue asterisks represent the $H\alpha$ emitting sources from Ogura et al. (2002) and large open circles $H\alpha$ sources from Nakano et al. (2012). The error bars in the left corners show the average errors in the colors. The thin and thick solid curves represent the unreddened main-sequence and giant branches (Bessell & Brett 1988), respectively. The dotted line indicates the locus of intrinsic CTTSs (Meyer et al. 1997). The parallel dashed lines are the reddening vectors drawn from the tip (spectral type M4) of the giant branch (“upper reddening line”), from the base (spectral type A0) of the main-sequence branch (“middle reddening line”)

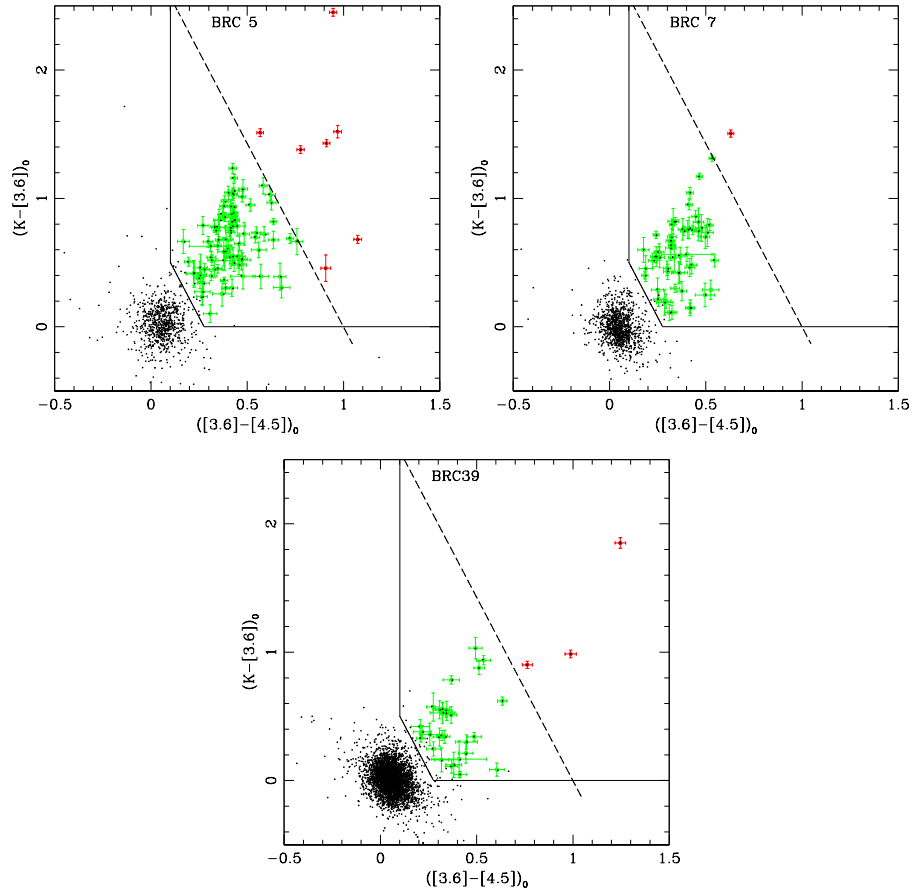


Figure 3. 2MASS – IRAC colour-colour diagrams for (a) BRC 5, (b) BRC 7 and (c) BRC 39. Red squares are class I sources and green circles are class II sources. The error bars in the left corners show the average errors in the colors.

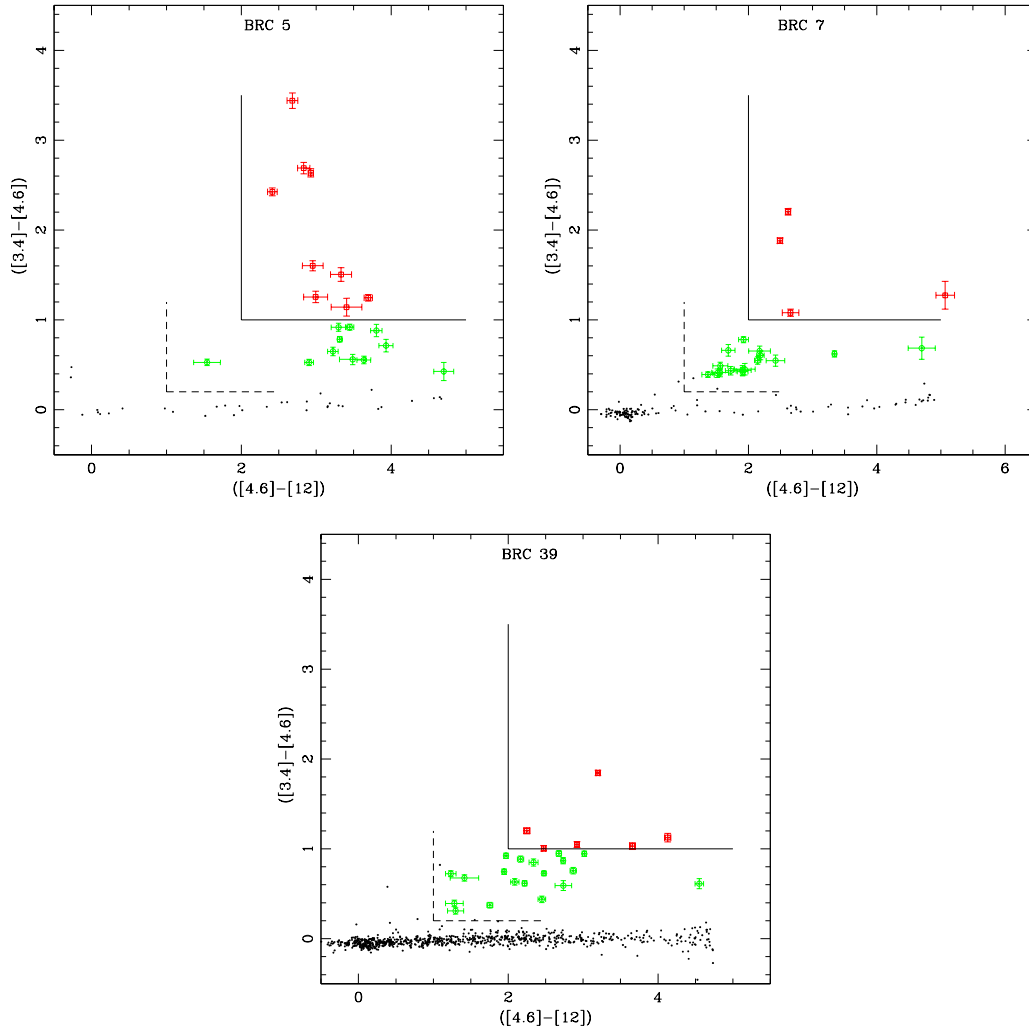
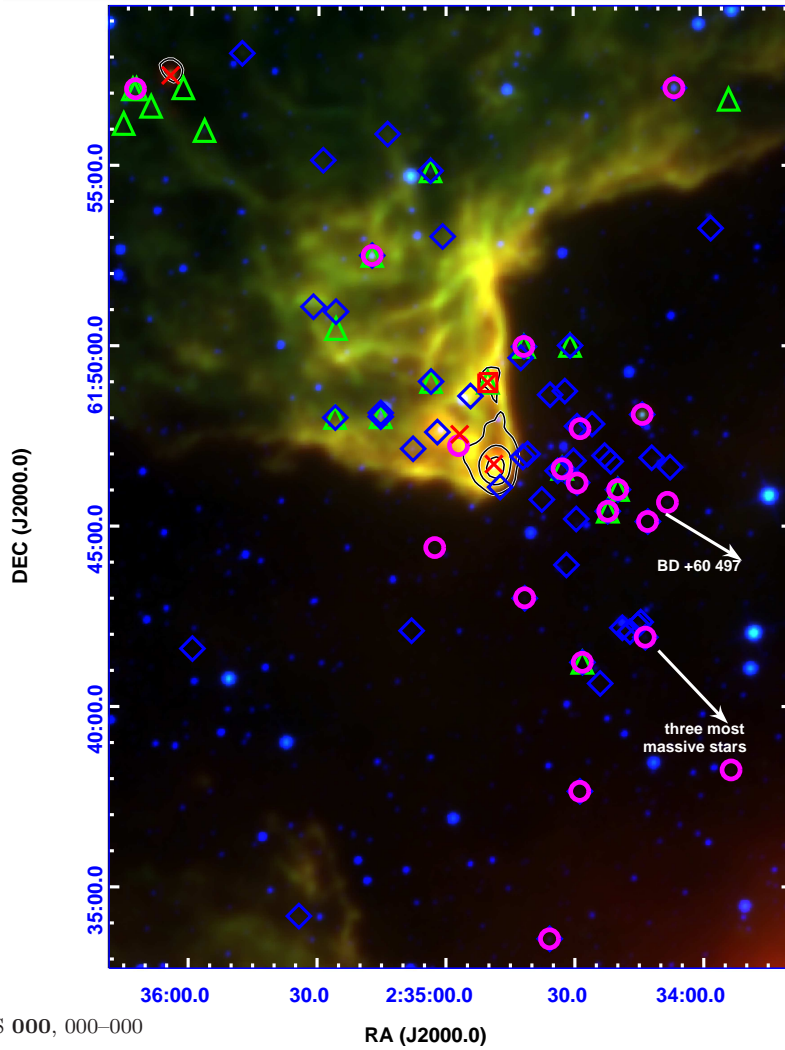
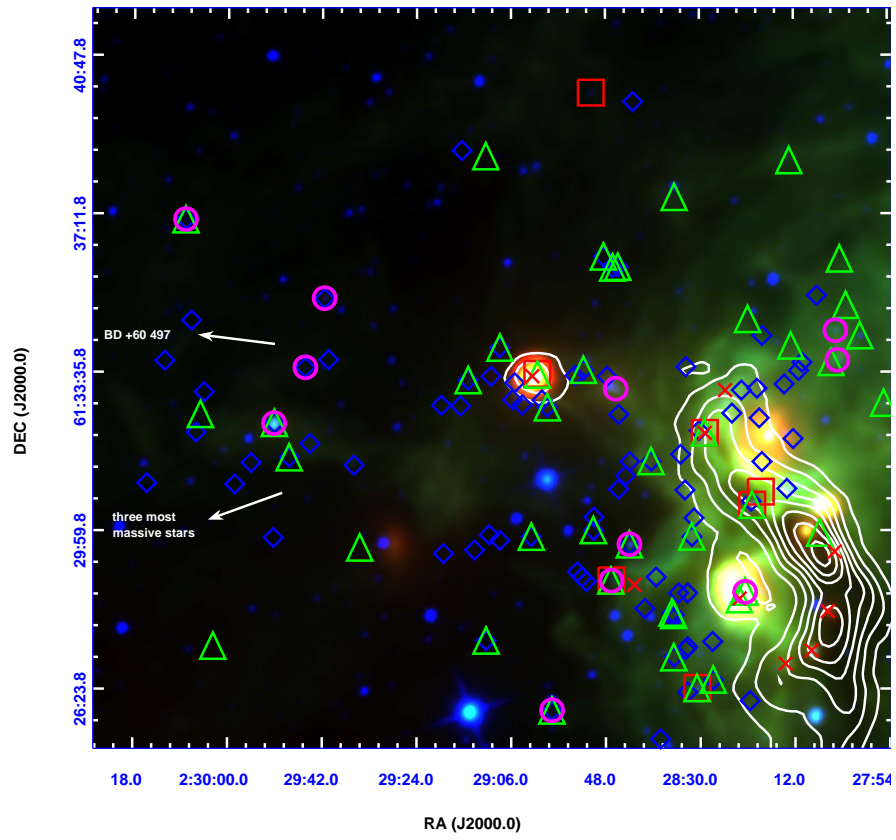


Figure 4. WISE two-colour diagram for selected YSOs in (a) BRC 5, (b) BRC 7 and (c) BRC 39 regions. Green circles represent class II sources and red squares represent class I sources. The error bars in the left corners show the average errors in the colors.



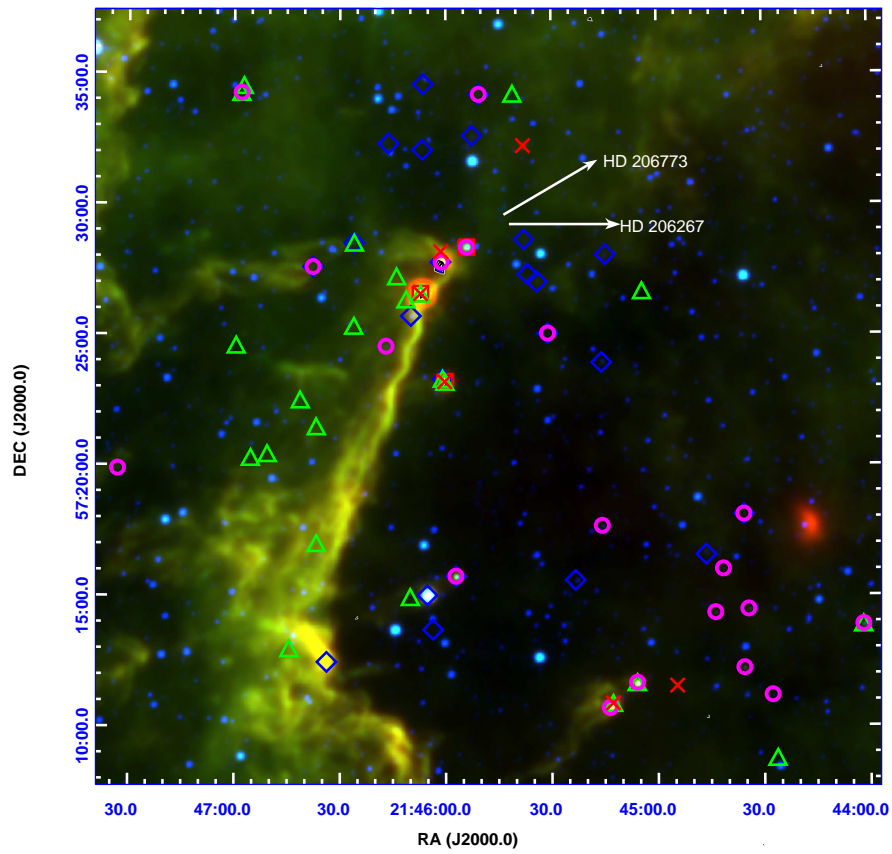


Figure 5. Spatial distribution of YSOs in (a) BRC 5, (b) BRC 7, (c) BRC 39 regions. Open triangles represent IR excess sources from 2MASS, Squares and diamonds represent the IRAC Class I and Class II sources respectively. Class I and Class II sources selected based on the WISE colors are shown as crosses and open circles, respectively. The contours represent the 1.1 mm emission obtained from the CSO BOLOCAM images

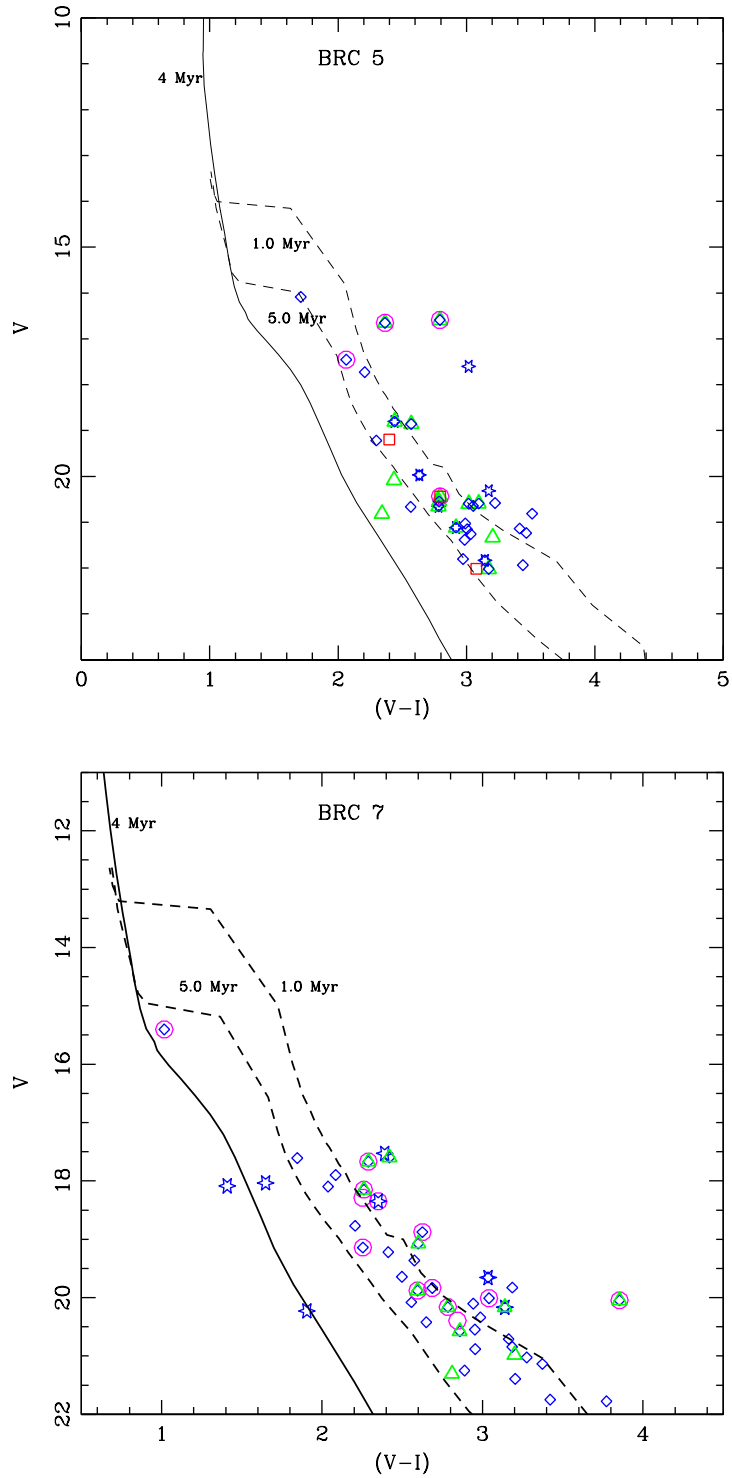


Figure 6. Optical $V/(V-I)$ colour-magnitude diagram of the (a) BRC 5, (b) BRC 7. Open triangles represent IR excess sources from 2MASS, squares and diamonds represent the IRAC Class I and Class II sources respectively. Class I and Class II sources selected based on the WISE colors are shown as crosses and open circles, respectively. Star symbols represents the position of H α emission stars (Ogura et al. 2002) and open triangle represent the IR excess sources from 2MASS.

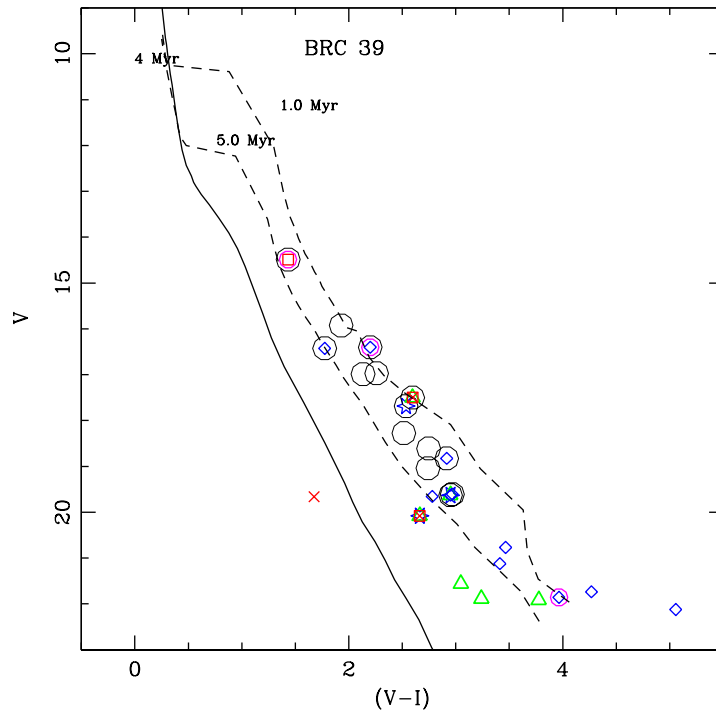


Fig. 6 cont. (c) BRC 39 region. Large open circles are the $H\alpha$ sources from Nakano et al. (2012). Other symbols are same as in previous figures.

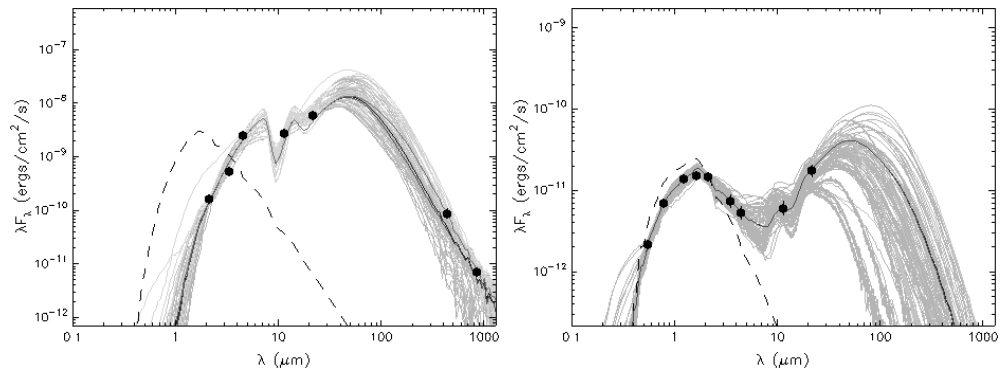


Figure 7. Sample SEDs for class I and class II sources in BRC 5. The dashed line shows the stellar photosphere corresponding to the central source of the best-fitting model. The grey lines show subsequent good fits to the data points, and the black line shows the best fit. The filled circles denote the input flux values.